applied sciences

MDPI

Communication

Solution-Processed Environmentally Friendly Ag_2S Colloidal Quantum Dot Solar Cells with Broad Spectral Absorption

Viktor A. Öberg, Xiaoliang Zhang, Malin B. Johansson and Erik M. J. Johansson *

Department of Chemistry-Ångström, Physical Chemistry Uppsala University, 75120 Uppsala, Sweden; viktor.oberg@kemi.uu.se (V.A.Ö.); xiaoliang.zhang@kemi.uu.se (X.Z.); malin.johansson@kemi.uu.se (M.B.J.)
* Correspondence: erik.johansson@kemi.uu.se

Received: 31 August 2017; Accepted: 29 September 2017; Published: 3 October 2017

Abstract: A facile heat-up synthesis route is used to synthesize environmentally friendly Ag_2S colloidal quantum dots (CQDs) that are applied as light absorbing material in solid state p-i-n junction solar cell devices. The as-synthesized Ag_2S CQDs have an average size of around 3.5 nm and exhibit broad light absorption covering ultraviolet, visible, and near infrared wavelength regions. The solar cell devices are constructed with a device architecture of FTO/TiO_2/Ag_2S CQDs/hole transport material (HTM) /Au using a solution-processed approach. Different HTMs, N2,N2,N2′,N2′,N7,N7,N7′,N7′-octakis(4-methoxyphenyl)-9,9′-spirobi(9H-fluorene)-2,2′,7,7′ tetramine (spiro-OMeTAD), poly(3-hexylthiophene-2,5-diyl) (P3HT), and poly((2,3-bis(3-octyloxyphenyl)-5,8-quinoxalinediyl)-2,5-thiophenediyl) TQ1 are studied for maximizing the device photovoltaic performance. The solar cell device with P3HT as a hole transport material gives the highest performance and the solar cell exhibit broad spectral absorption. These results indicate that Ag_2S CQD have high potential for utilization as environmentally friendly light absorbing materials for solar cell application and that the hole transport material is critical to maximize the solar cell photovoltaic performance.

Keywords: quantum dot; Ag_2S; solar cell; low-toxic; energy conversion

1. Introduction

Solar cell technology for energy conversion has been on the rise in the past decades, mainly due to the challenges of global climate change and, consequentially, the need to decrease the usage of fossil fuels. A lot of effort has been put into inquiries of photovoltaic devices, where the aim is to convert solar energy into electrical current. The common long term goal of this research is to find a combination of materials in a solar cell device which has low cost, short energy payback time, abundant materials, that is stable and highly efficient. One of these solar cell systems is the third generation quantum dot solar cells (QDSC). In 2002, some of the device structures seen today for QDSCs were proposed [1]. Since then, different types of QDSCs have been investigated including p-i-n junction solar cells [2–11], quantum dot sensitized solar cells (QDSCs) [12–16], and QD-polymer solar cells [17]. State of the art PbS QDSCs achieves most of goals stated above with efficiencies currently around 11.3% [5]. However, there is one last criterion which gets increasingly more important and that is environmental sustainability and more specifically toxicology. The industrial usage of lead in solar cells will increase the demand in handling, manufacturing, and waste handling in production of these devices. Thus, to avoid these risks, choosing a material with low-toxicity and that is more environmentally friendly becomes important. One of these potential materials is Ag_2S.

Ag_2S is a mid-range band gap semiconductor with a band gap of about 1 eV and it has a rather large light absorption coefficient making it a promising candidate in photovoltaic applications. It has

been shown that the band gap can be increased to at least 1.1 eV (1120 nm) by decreasing the size of the nanocrystals to about 3 nm, due to relatively weak quantum confinement effects [18,19]. A few studies have been made on Ag_2S as an inorganic light-absorber. The stability of Ag_2S quantum dots produced by successive ionic layer adsorption and reaction (SILAR) as well as their ability to inject electrons into an n-type semi-conductor, such as TiO_2, have been investigated [20]. Above 1% solar to electricity power conversion efficiency (PCE) using a device structure similar to the dye-sensitized solar cells has been achieved [21–24]. However, there have been no reports on solar cells based on solid CQD layers with Ag_2S, similar to the solid CQD layers used in the most efficient PbS CQD solar cells discussed above. In this report, we therefore investigate solar cell device based on Ag_2S CQD solids, and specifically investigate the influence of the hole transport material (HTM) in the device.

There are a few methods to produce the Ag_2S quantum dots. A hot-injection method can be deployed as it is known to give a large amount of quantum dots with a low polydispersity and high yield. This can be done in polar and non-polar solvents, providing quantum dots with a non-polar ligand. This method is common for many other materials such as CdS and PbS [25,26]. However, this method is difficult to implement at an industrial level as the injection of sulphur precursor is usually performed at a timescale of around a second, which becomes increasingly more difficult at larger volumes. The heat-up synthesis can therefore be advantageous due to its simplicity, and the potential to more easily upscale the synthesis and that the properties (e.g., size and optical properties) from batch to batch are very similar [27].

In this study, the heat-up approach was applied to synthesize Ag_2S CQDs for the application in solar cells with a p-i-n heterojunction architecture.

The solar cells in this work are prepared using a solution-based approach under ambient condition. A thin layer of n-type TiO_2 is used as an electron transport layer. Different hole transport materials (HTMs) with different energy levels, such as poly(3-hexylthiophene-2,5-diyl) (P3HT), N2,N2,N2′,N2′,N7,N7,N7′,N7′-octakis(4-methoxyphenyl)-9,9′-spirobi 9H-fluorene-2,2′,7,7′-tetramine (spiro-OMeTAD) and poly((2,3-bis(3-octyloxyphenyl)-5,8-quinoxalinediyl)-2,5-thiophenediyl) (TQ1) are studied to maximize the solar cell efficiency. The results show that the energy level of HTM is critical for the hole extraction and therefore also the solar cell photovoltaic performance since the gold contact might not be selective towards any of the charge carriers [28].

2. Experimental Section

2.1. Chemicals

AgNO3 (≥99.8%), dodecanethiol (98%), ethanol (99.98%), acetonitrile (ACN) (99.8%), Ti(IV)-isopropoxide (97%), isopropanol (99.9%), acetylacetone (≥99.5%), $TiCl_4$ (99.9%), P3HT (99.995%), TQ1, 4-tert-butylpyridine (96%), chlorobenzene (99.8%), , LiTFSI (99%), methanol (≥99.9%), toluene (99.8%), 3-mercaptopropionic acid (≥99.0%), and ethanedithiol (EDT) (≥98%) were bought from Sigma-Aldrich, Saint Louis, MO, USA and used as described. tris(2-((1H-pyrazol-1-yl)-4-tert-butylpyridine)cobalt(III) tris(bis(trifluoromethylsulfonyl)imide)) (>95%) was bought from Dyenamo, Stockholm, Sweden, Spiro-OMeTAD (99.5%) was bought from Borun New Material Technology Ltd., Ningbo, China, and cyclohexane (99.5%) was bought from Merck and used as described. FTO-covered glass with a resistance of 15 Ω/□ is produced by Pilkington and bought from Hartford Glass Co., Inc, Hartford City, IN, USA.

2.2. CQD Synthesis

Ag_2S colloidal quantum dots (CQDs) were synthesized according to literature [27] with some modification. In short, 680 mg (4 mmol) AgNO3 and 33.8 g (40 mL) dodecanethiol (DT) was placed in a 100 mL three-necked flask. The flask was put in a pre-heated 215 °C silicon oil bath. The oil bath temperature decreased to 210 °C and was kept at this temperature during the whole reaction of 21 min. The temperature of the mixture in the flask quickly increased to around 185 to 190 °C at a rate

between 25 and 30 °C/min. Thereafter the temperature continued to increase more slowly up to 200 °C. The reaction was held at 200 °C for the rest of the reaction for a total reaction time of 21 min. The color of the mixture changed as it was heated and as the reaction was occurring. Below 120 °C, the color of the mixture was an orange-red. At 130 °C, the color of the mixture changed to yellow. Ending the reaction here would only yield insoluble silver thiolate. At 170 to 180 °C the solution darkened to a light orange and as the reaction was heated further to 200 °C and kept there, the solution darkened further. At the end of the reaction, the color was dark red upon at which time the reaction was cooled in a 0 °C ice bath. While cooling, the solution turned red-brown and murky as the dots grew to their final size and silver thiolate started to precipitate. An ice bath was used as it was shown that a higher cooling rate was important for the quality of the end product, especially the yield.

The dispersion of CQDs was centrifuged at 4000 rpm for 4 min. The silver thiolate byproduct formed a solid precipitate on the bottom while the quantum dots were still dispersed in the liquid phase. After discarding the thiolate, acetonitrile, and ethanol was used for precipitation of the CQDs and the dispersion was centrifuged for 4 min at 4000 rpm. The liquid was removed and the nanocrystals were dried upside down for ca 30 min. Cyclohexane was used to disperse the dots followed by a new addition of acetonitrile and ethanol. Once again, the mixture was centrifuged at 4000 rpm for 4 min to collect the dots. This was repeated once more, after which the dots were finally dispersed in cyclohexane and filtered through a filter with a pore size of 200 nm. The amount of quantum dots for such a reaction described above yielded between 150 to 250 mg.

2.3. Solar Cell Fabrication

For all samples, a compact TiO_2 layer was applied and used as the electron acceptor (electron transport layer) on conductive fluorine doped tin oxide (FTO). In short, the TiO_2 layer was applied through spray pyrolysis at 550 °C using an isopropanol solution containing 2 M acetylacetone and 0.2 M Ti(IV)-isopropoxide as a precursor. The films were then bathed in $TiCl_4$ (120 mM) for 30 min at 70 °C, before being cleaned, dried, and sintered again at 500 °C. When not in use, the TiO_2 films were stored in a dry oven at 120 °C.

The Ag_2S CQDs were diluted to 30 mg/mL and then spin-coated using a KW-4A Chemat Technology spin-coater onto the TiO_2 film following a layer-by-layer method. The CQDs were first spin-coated, and thereafter a solution of 0.01 vol % ethanedithiol (EDT) in acetonitrile was applied on the CQD layer. The EDT solution coated the CQD layer for 30 s to exchange the ligands before the device was spun again. The film layer was then washed with acetonitrile twice or with methanol and toluene. The speed was 600 rpm for 3 s followed by 2000 rpm for 30 s for all steps. The process was repeated again until the desired thickness, usually between 3 to 12 layers (see Scheme 1), was obtained. Since the CQDs were not washed away during the cleaning step, it can be concluded that the ligands on the QD at least partly are exchanged to EDT in the film. 3-mercaptopropionic acid (3-MPA) was also tested as a linker in the ligand exchange to obtain a CQD film. However, for the (3-MPA) the formed films were not very stable and washed away during the cleaning step, suggesting that the carboxylic acid group did not bind to the CQDs, meaning that the 3-MPA did not work as a linker in this case (see Supplementary Materials). We therefore use EDT as the linker in this work. Some of the devices were then spin-coated with a layer of doped Spiro-OMeTAD or P3HT as a hole transport material (HTM) for 3 s at a speed of 600 rpm followed by 3000 rpm for 40 s. Lastly, a 80 nm thick gold layer was deposited on the HTM using a LEICA EM MED020 evaporator to complete the device.

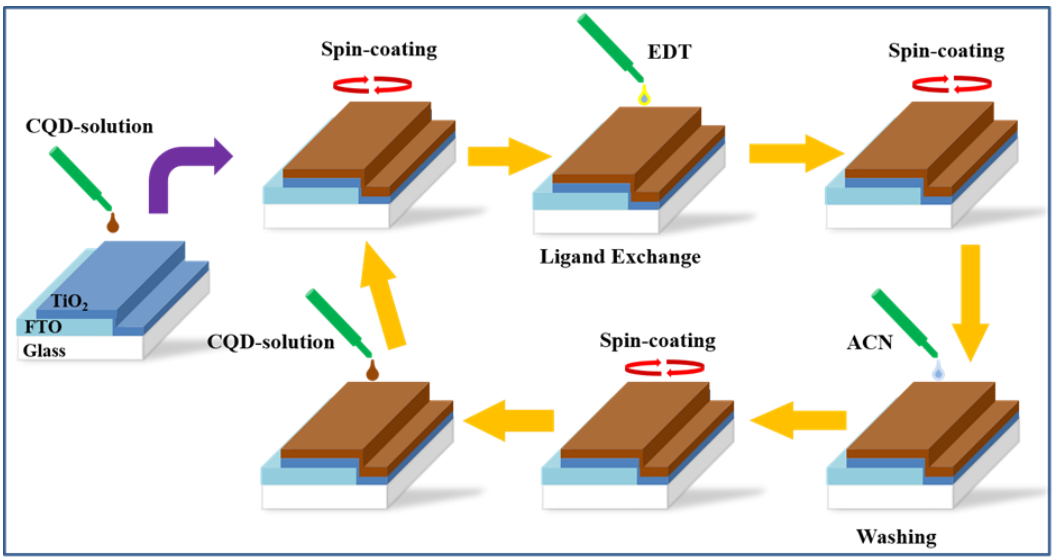

Scheme 1. The process of making the CQD films using a layer-by-layer method. The CQD dispersion was first spin-coated on top of bare TiO_2 (as denoted by the purple arrow), followed by ligand exchange with the linker EDT and washing twice using pure solvents. The process was then repeated until the desired thickness was achieved.

3. Results and Discussion

3.1. CQD Properties

The light absorption spectrum of the synthesized quantum dots was measured using a DH-2000 BAL Mikropak deuterium and halogen lamp source combined with an Ocean Optics detector and is shown in Figure 1a. The concentration of CQDs was 0.5 mg/mL. The CQDs show a broad light absorption from UV, through the entire visible region and further extending in the near IR region. As can be seen in the spectrum, the Ag_2S CQDs do not display an excitonic peak. Instead, there is a shoulder at 820 nm, corresponding to a peak in the second derivative spectrum (Figure S1). Also in Figure 1a, the photoluminescence spectrum, measured using a Horiba Jobin Yvon FluoroLog modular fluorospectrometer is shown. The spectrum shows a peak at 965 nm with a faint shoulder at 906 nm (Figure S2) and a 'blue' tail. The concentration of this sample was 2 mg/mL, as seen in the right vial in Figure 1b. In Figure S3, a similar photoluminescence spectrum can be seen. It shows the emission of a thin spin-coated film of the CQDs.

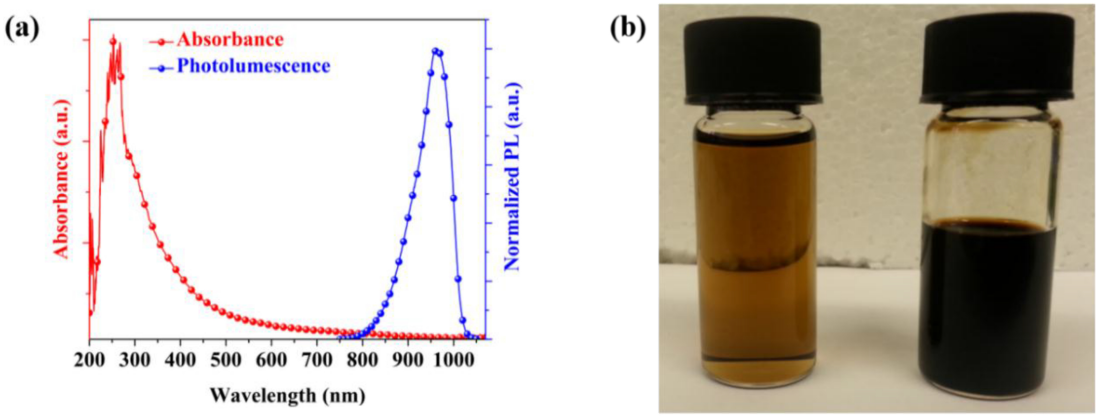

Figure 1. *Cont.*

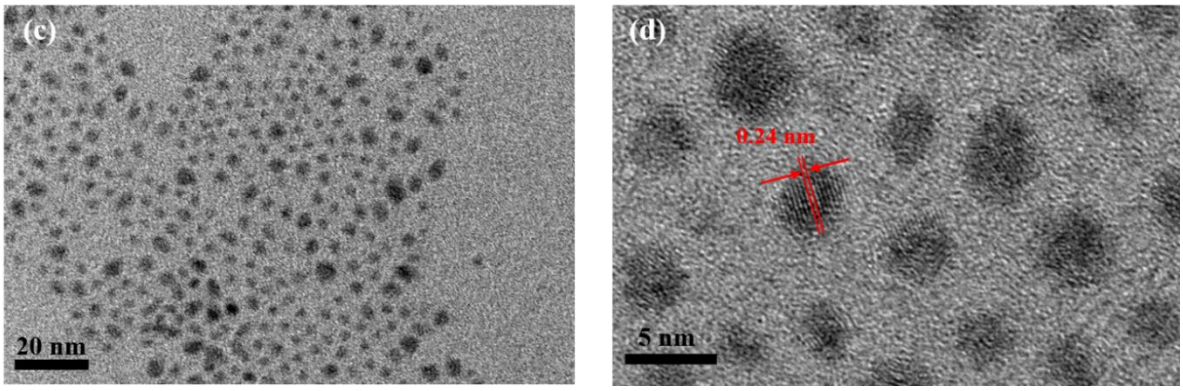

Figure 1. (**a**) Shows the absorbance spectrum of a 0.5 mg/mL Ag_2S dispersion and a normalized PL emission spectrum of a 2 mg/mL Ag_2S dispersion. The PL spectrum was excited with a wavelength of 550 nm; (**b**) Shows QDs at different concentrations: 2 mg/mL (left) and 30 mg/mL (right); (**c**) Shows a TEM image of the synthesized nanocrystals, while (**d**) is an HR-TEM image of the same sample, showing the distance between two planes in one of the crystals.

The CQDs were studied using a field emission transmission electron microscope (FE-TEM) JEOL (Model JEM-2100F) with electron diffraction function, operated at 200 kV and with probe size under 0.5 nm. Figure 1c,d were analyzed to assess the size and morphology of the Ag_2S CQDs. The average size calculated from Figure S4 was 3.59 nm and this sample's histogram is shown in the Figure S5. The CQDs are all below the size of 8 nm and the average size is lower than 4 nm, which has been proposed as the size below which strong quantum confinement effects change the absorption properties of the nanocrystals [18]. This is further confirmed by absorbance and photoluminescence studies (see Figure 1a) in which absorption ends around 1000 nm and an emission peak at 975 nm is seen, showing that the electrons are confined as compared to bulk Ag_2S. It is notable that the Ag_2S CQD dispersion is rather stable and almost no aggregation occurred over periods of months under ambient conditions after synthesizing them.

Figure S6 shows a FFT-pattern of a single monoclinic crystal and was measured using the FE-TEM. The FFT-pattern shows how the distances between planes in the reciprocal lattice are related to one another. The distances were measured and the ratios were calculated and compared to theoretical lattice parameters found in literature [29]. Matching these parameters supports our suggestion that the synthesized nanocrystals are monoclinic Ag_2S. X-ray diffraction conducted on thiol-capped Ag_2S nanoparticles shows similarity in shape to a theoretical standard diffractogram, even though the peaks are broad due to particle size broadening and Ag_2S being monoclinic (Figure S7). In Figure 1d, the distance d between two planes in a crystal is shown. This distance corresponds to $2\theta = 37.4^\circ$ in the diffractogram in Figure S7 using Bragg's law.

3.2. Solar Cell Characterization

In Figure 2a, the device architecture is shown with the different layers in the device, and Figure 2b shows a cross-sectional image of a CQD solar cell device using a Zeiss 1550 scanning electron microscope (SEM) with at an accelerating voltage of 5 kV. From the SEM cross section, the TiO_2 layer was estimated to be ~60 nm (six layers), the thickness of the quantum dot layer is ~108 nm, and the thickness of the P3HT layer is 80 nm, and the gold layer is 80 nm.

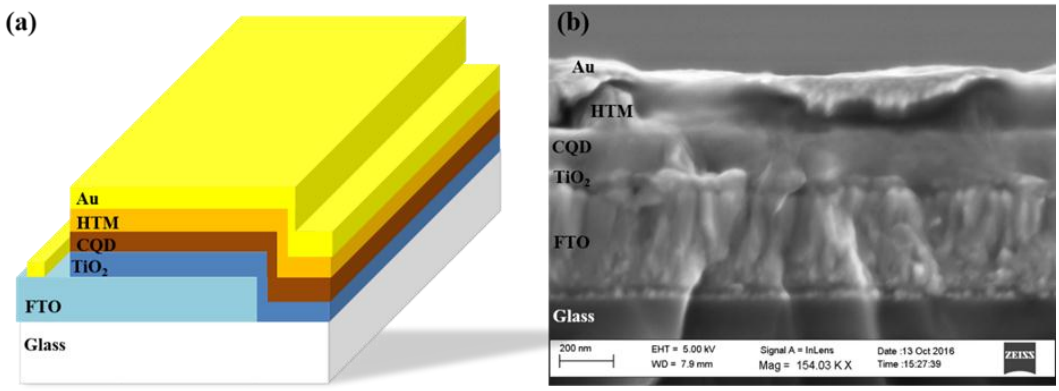

Figure 2. (**a**) Shows a schematic representation of a finished device and (**b**) is the SEM cross section of a real device with the different layers labeled.

Figure 3a shows the absorption spectra of samples with glass/FTO/TiO_2 and a CQD film with a layer of spiro-OMeTAD, a CQD film with a layer of P3HT and films with P3HT and spiro-OMeTAD. Comparing the absorption of the CQD film (Figure 3a) and the CQD solution (Figure 1a) the light absorption spectra are rather similar, with light absorption extending to around 900 nm. For the CQD film with P3HT, there is a slight enhanced absorption in the 450 to 650 nm region due to the P3HT layer. Many of the features in the IR region of the spectra of the films with only P3HT and only spiro-OMeTAD are difficult to interpret. This is due to interference effects of the very thin films as well as reflection from the TiO_2.

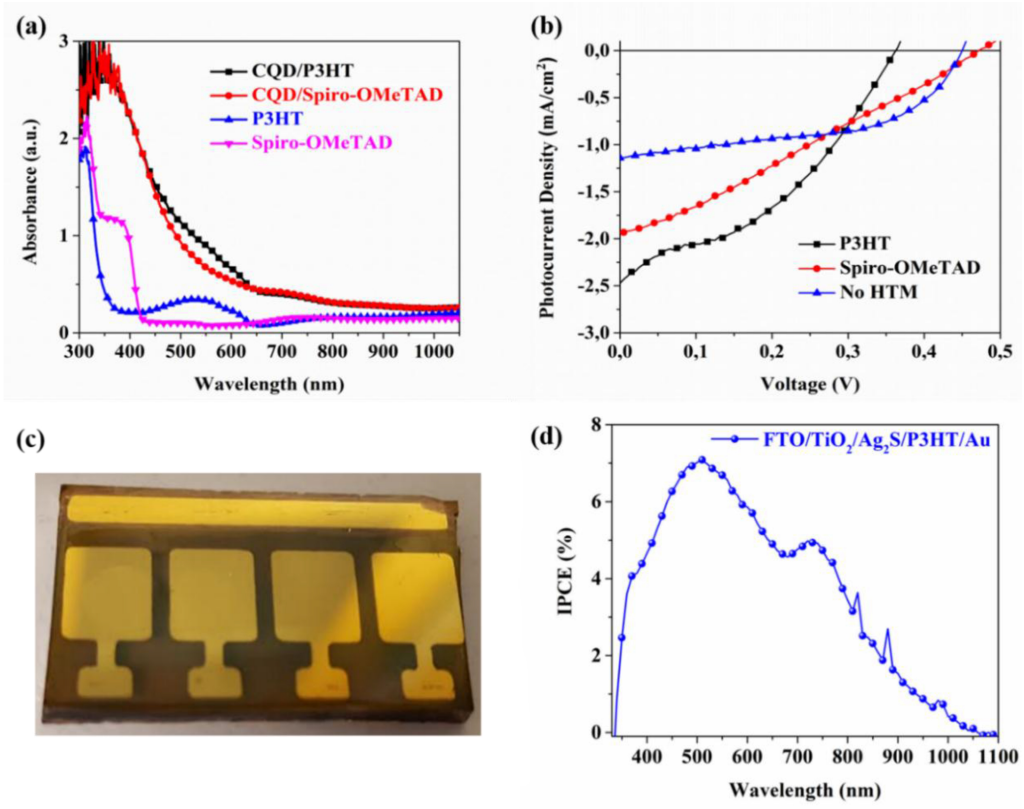

Figure 3. (**a**) Shows the absorbance of HTMs with and without QDs. The films are of incomplete devices on which only the gold layer is missing; (**b**) Shows JV curves of the best devices made; (**c**) Shows an image of a device; (**d**) Is the IPCE of a solar cell device with P3HT as the HTM. The peaks between 800 and 900 nm are residual peaks from the Xe lamp.

3.3. Device Performance

Photovoltaic performance of the Ag_2S CQD solar cells with P3HT and spiro-OMeTAD HTM layers, and without any HTM layer were measured using a solar simulator with AM1.5G 100 mW/cm^2 illumination from a Newport Xe lamp combined with a Keithley 2400 Sourcemeter. The working area of the solar cells was 0.126 cm^2 as defined by a black metallic aperture.

The resulting J–V curves for the best solar cells are displayed in Figure 3b and the resulting photovoltaic parameters, such as short-circuit current density (Jsc), open-circuit voltage (Voc), fill factor (FF) and PCE, and are summarized in Table 1 (see Supplementary Materials for non-rounded data). The best cell with P3HT as a HTM was constructed with a CQD solid of six CQD layers and the best cell without any HTM was constructed with a CQD solid of nine CQD layers, and the best cell with spiro-OMeTAD was constructed with four CQD layers. Comparing the results, it can be concluded that the HTM has a strong influence on the device characteristics. The CQD solar cells with P3HT as a HTM show higher photocurrent but slightly lower photovoltage, while the CQD solar cells with spiro-OMeTAD HTM show higher photovoltage and slightly lower photocurrent. The solar cells with no HTM show much lower current, but relatively high voltage.

We can therefore conclude that for the devices with a HTM layer a larger photocurrent can be obtained, which indicates that the HTM is important in the extraction of the holes from the CQD layer. At the same time the photovoltage is affected by the HTM, which may be a result of either different charge extraction efficiency or different recombination rate of the photogenerated charges for the devices with different HTMs. The charge extraction and charge recombination at the CQD/HTM interface depends on the energy levels and molecular structure at the interface and can be affected both by the individual properties of the materials, but also on the interaction between the HTM and the CQD layer [28,30].

The J–V curve for the P3HT based device shows a slight s-shape close to short-circuit. This has been obtained for several of the tested devices, and indicates that there is a barrier for charge extraction in the devices, and the IPCE results further down, using an ASB-XE-175 Xe light source connected to a Spectral Products monochromator and AB300 series controller, suggests that the TiO_2/CQD interface may limit the device performance.

The fabricated devices (see Figure 3c) show a promising voltage up towards 0.5 V, but have a very low current and fill factor, which limits the efficiency drastically. J–V measurements in the dark (Figure S8) show that the devices are limited by a considerable dark current, which indicates that the recombination at the interfaces in the device is very important. As seen in Figure S8, P3HT has a lower dark current than spiro-OMeTAD.

Table 1. Device parameters from the devices shown in Figure 3b.

HTM	V_{OC} (V)	J_{SC} (mAcm^{-2})	FF	Eff. (%)
Spiro-OMeTAD	0.47	−1.9	0.28	0.25
P3HT	0.37	−2.5	0.38	0.34
-	0.45	−1.1	0.52	0.27

Further, the IPCE spectrum (see Figure 3d), shows a broad photocurrent response. This is in agreement with the broad absorption spectrum of the Ag_2S CQDs, and shows the potential for utilization of a large part of the solar spectrum with solar cells based on Ag_2S CQDs. In the device the light with short wavelength is absorbed close to the TiO_2 layer and light with longer wavelength is absorbed closer to the HTM layer, since the Ag_2S CQDs have larger light absorption in the short wavelength region (compare Figure 1a, Figure 3a,d). The rather low efficiencies obtained in the devices we therefore relate to the TiO_2/CQD interface and further enhancement of the device efficiency should in future be focused on this interface.

The two HTMs that are investigated in this study have been used extensively in many different solar cell devices ranging from polymer solar cells, to hybrid perovskite solar cells, to quantum dot solar cells [30–37]. P3HT has been reported to have its highest occupied molecular orbital (HOMO) and lowest unoccupied molecular orbital (LUMO) levels at −5.1 and −2.9 eV respectively [34,38], while spiro-OMeTAD has its HOMO level at −5.22 eV [28]. The P3HT in this study was undoped, while spiro-OMeTAD was doped with cobalt and lithium (see Supporting Information (SI)) according to previous studies to lower the Fermi level and increase the conductivity [39]. A third hole conductor, poly((2,3-bis(3-octyloxyphenyl)-5,8-quinoxalinediyl)-2,5-thiophenediyl) (TQ1), was also investigated in this study, as it has been shown to take a similar role as P3HT in organic polymer solar cells [40]. However, using TQ1 did not result in any comparable voltage and thus no efficiency was measured, see Figure S9.

As mentioned before, different thicknesses of the CQD layers were investigated. In the case of spiro-OMeTAD, three, four, six, and eight layers of CQDs were investigated, were four layers gave the highest efficiency as seen in Figure S10a–c. While the four layer cell had the highest efficiency, the fill factor is very low, which can be attributed to pin holes in the very thin film. For thicker CQD films (six and eight layers) the solar cells show a higher fill factor, but the photovoltage and photocurrent are lower and the series resistance increases in the devices, which decreases the overall efficiency drastically. Important to note that also the thickness of TiO_2 was investigated with an optimal thickness around 60 nm.

P3HT was investigated at thicknesses of six layers of CQDs, which gave the record efficiency (see Figure 3b). However, at a separate occasion different thickness of the Ag_2S CQD layer was investigated (6, 9, and 12 layers), were the efficiency was comparably similar for all thicknesses (see Figure S10d).

For no HTM, cells with six and nine layers were investigated, were the one with nine layers gave the highest efficiency (Figure S11). The thickness of the CQD layer was therefore found to influence the efficiency of the devices, and depending on the HTM, a different optimal thickness was obtained. This can be due to the limited transport length or diffusion length of the photogenerated charges in the CQD layer, and the ability of the HTMs to extract the holes from the CQD layer. Comparing spiro-OMeTAD and P3HT based devices with the same CQD layer thickness (six layers of CQDs, see Supporting Information), we observe a higher photocurrent from the P3HT based device, which again confirms the more efficient hole extraction with P3HT. If the hole extraction from the CQD layer is efficient a thicker CQD layer may be used, compared to for a less efficient hole extraction layer, however at the same time the charge recombination at the HTM/CQD interface must be considered, which may also differ for different HTMs. Also the maximum thickness of the CQD layer is dependent on the electron extraction from the CQD layer to the TiO_2 layer. As mentioned above, the IPCE spectrum indicates that the electron extraction is not optimal, and the overall rather low currents from the solar cells also suggests that the electron extraction is not optimal.

While the CQD dispersion stability is high and it has been possible to store the CQD dispersion for several months without a considerable change in its soluble and optical properties, the CQD films are unstable under strong illumination, resulting in bleaching of the device, especially during measurements. As previous studies have reported Ag_2S as being highly stable even in working devices under illumination [22], this photo instability can be attributed to the specific conditioning of the nanocrystals during spin-coating them into the film. We therefore think that the device instability is linked to the surface ligand of the CQDs used in the solar cells. One possibility is that with EDT as the linker, the ligand exchange is too slow, causing a mixture of ligands (DT) and linkers (EDT) on the surface. This may cause unwanted surface properties and instability of the CQD films. The aforementioned instability has limited the amount of times each device can be measured and is possibly also another reason for the rather low efficiencies obtained. The bleached area of the devices most probably contain metallic silver as the color is usually greenish silver (see Supporting Information). Since no degradation was found for the CQDs before ligand exchange, we can conclude

that finding a different ligand for the CQD dispersion that is stable but also easily exchangeable for linkers is essential in future development of these devices.

4. Conclusions

The Ag_2S CQDs were synthesized using a versatile method with the resulting nanocrystals being nonpolar and highly soluble at high concentrations in cyclohexane. The solid-state solar cells with Ag_2S CQD solid as a light absorber were fabricated using a solution-processed method, and the solar cell devices show broad light absorption. A HTM layer with suitable energy levels is critical for the solar cell photovoltaic performance that diminish the interfacial recombination at CQD/Au interface. The solar cell with P3HT as hole transport material gives a promising efficiency and a broad spectra response from the UV to the near IR region of the solar spectrum. These results therefore indicate that Ag_2S CQDs are promising for further development toward environmental friendly solar cells or other optoelectronic devices.

Supplementary Materials: The following are available online at www.mdpi.com/2076-3417/7/10/1020/s1. Figure S1: 2nd derivative of the absorbance spectrum, Figure S2: 2nd derivative of the photoluminescence spectrum, Figure S3: Normalized PL emission spectrum of CQD film, Figure S4: TEM image, Figure S5: Size distribution of the Ag_2S quantum dots, Figure S6: FFT pattern of 1 single quantum dot crystal, Figure S7: Experimental and theoretical X-ray diffractogram, Figure S8: J-V curves of P3HT and spiro-OMeTAD cells in the dark, Figure S9: J-V curve of solar cell with TQ1 as the HTM, Figure S10: J-V-curves of several devices made by using Spiro-OMeTAD and P3HT as an HTM, Figure S11: J-V-curves of the best devices using no HTM, Table S1: Comparison between this study's ratios of the reciprocal lattice constants, Table S2: Non-rounded parameters of the best cell efficiencies.

Acknowledgments: This work was funded by Swedish Energy Agency, Göran Gustafsson Foundation, ÅForsk, the Swedish Research Council FORMAS and Swedish Research Council (VR). The authors thank G. Boschloo and L. Häggman for discussions and technical support.

Author Contributions: V.A.Ö. and E.M.J. conceived and designed the experiments; V.A.Ö., M.B.J. and X.Z. performed the experiments; V.A.Ö, M.B.J, X.Z., E.M.J. analyzed the data; V.A.Ö., M.B.J., X.Z, E.M.J contributed reagents/materials/analysis tools; V.A.Ö., E.M.J. wrote the paper.

Conflicts of Interest: The authors declare no conflict of interest.

References

1. Nozik, A.J. Quantum dot solar cells. *Phys. E Low-Dimens. Syst. Nanostruct.* **2002**, *14*, 115–120. [CrossRef]
2. McDonald, S.A.; Konstantatos, G.; Zhang, S.; Cyr, P.W.; Klem, E.J.D.; Levina, L.; Sargent, E.H. Solution-processed pbs quantum dot infrared photodetectors and photovoltaics. *Nat. Mater.* **2005**, *4*, 138–142. [CrossRef] [PubMed]
3. Zhang, J.; Gao, J.; Church, C.P.; Miller, E.M.; Luther, J.M.; Klimov, V.I.; Beard, M.C. Pbse quantum dot solar cells with more than 6% efficiency fabricated in ambient atmosphere. *Nano Lett.* **2014**, *14*, 6010–6015. [CrossRef] [PubMed]
4. Semonin, O.E.; Luther, J.M.; Choi, S.; Chen, H.-Y.; Gao, J.; Nozik, A.J.; Beard, M.C. Peak external photocurrent quantum efficiency exceeding 100% via meg in a quantum dot solar cell. *Science* **2011**, *334*, 1530–1533. [CrossRef] [PubMed]
5. Liu, M.; Voznyy, O.; Sabatini, R.; Garcia de Arquer, F.P.; Munir, R.; Balawi, A.H.; Lan, X.; Fan, F.; Walters, G.; Kirmani, A.R.; et al. Hybrid organic-inorganic inks flatten the energy landscape in colloidal quantum dot solids. *Nat. Mater.* **2017**, *16*, 258–263. [CrossRef] [PubMed]
6. Kramer, I.J.; Minor, J.C.; Moreno-Bautista, G.; Rollny, L.; Kanjanaboos, P.; Kopilovic, D.; Thon, S.M.; Carey, G.H.; Chou, K.W.; Zhitomirsky, D.; et al. Efficient spray-coated colloidal quantum dot solar cells. *Adv. Mater.* **2015**, *27*, 116–121. [CrossRef] [PubMed]
7. Kramer, I.J.; Moreno-Bautista, G.; Minor, J.C.; Kopilovic, D.; Sargent, E.H. Colloidal quantum dot solar cells on curved and flexible substrates. *Appl. Phys. Lett.* **2014**, *105*, 163902. [CrossRef]
8. Kemp, K.W.; Labelle, A.J.; Thon, S.M.; Ip, A.H.; Kramer, I.J.; Hoogland, S.; Sargent, E.H. Interface recombination in depleted heterojunction photovoltaics based on colloidal quantum dots. *Adv. Energy Mater.* **2013**, *3*, 917–922. [CrossRef]

9. Zhitomirsky, D.; Kramer, I.J.; Labelle, A.J.; Fischer, A.; Debnath, R.; Pan, J.; Bakr, O.M.; Sargent, E.H. Colloidal quantum dot photovoltaics: The effect of polydispersity. *Nano Lett.* **2012**, *12*, 1007–1012. [CrossRef] [PubMed]
10. Ko, D.-K.; Brown, P.R.; Bawendi, M.G.; Bulović, V. P-i-n heterojunction solar cells with a colloidal quantum-dot absorber layer. *Adv. Mater.* **2014**, *26*, 4845–4850. [CrossRef] [PubMed]
11. Brown, P.R.; Lunt, R.R.; Zhao, N.; Osedach, T.P.; Wanger, D.D.; Chang, L.-Y.; Bawendi, M.G.; Bulović, V. Improved current extraction from zno/pbs quantum dot heterojunction photovoltaics using a moo3 interfacial layer. *Nano Lett.* **2011**, *11*, 2955–2961. [CrossRef] [PubMed]
12. Robel, I.; Subramanian, V.; Kuno, M.; Kamat, P.V. Quantum dot solar cells. Harvesting light energy with cdse nanocrystals molecularly linked to mesoscopic TiO_2 films. *J. Am. Chem. Soc.* **2006**, *128*, 2385–2393. [CrossRef] [PubMed]
13. Choi, H.; Radich, J.G.; Kamat, P.V. Sequentially layered cdse/cds nanowire architecture for improved nanowire solar cell performance. *J. Phys. Chem. C* **2014**, *118*, 206–213. [CrossRef]
14. Rühle, S.; Shalom, M.; Zaban, A. Quantum-dot-sensitized solar cells. *ChemPhysChem* **2010**, *11*, 2290–2304. [CrossRef] [PubMed]
15. Pan, Z.; Mora-Seró, I.; Shen, Q.; Zhang, H.; Li, Y.; Zhao, K.; Wang, J.; Zhong, X.; Bisquert, J. High-efficiency "green" quantum dot solar cells. *J. Am. Chem. Soc.* **2014**, *136*, 9203–9210. [CrossRef] [PubMed]
16. Wang, J.; Mora-Seró, I.; Pan, Z.; Zhao, K.; Zhang, H.; Feng, Y.; Yang, G.; Zhong, X.; Bisquert, J. Core/shell colloidal quantum dot exciplex states for the development of highly efficient quantum-dot-sensitized solar cells. *J. Am. Chem. Soc.* **2013**, *135*, 15913–15922. [CrossRef] [PubMed]
17. Dayal, S.; Kopidakis, N.; Olson, D.C.; Ginley, D.S.; Rumbles, G. Photovoltaic devices with a low band gap polymer and cdse nanostructures exceeding 3% efficiency. *Nano Lett.* **2010**, *10*, 239–242. [CrossRef] [PubMed]
18. Lin, S.; Feng, Y.; Wen, X.; Zhang, P.; Woo, S.; Shrestha, S.; Conibeer, G.; Huang, S. Theoretical and experimental investigation of the electronic structure and quantum confinement of wet-chemistry synthesized ag2s nanocrystals. *J. Phys. Chem. C* **2015**, *119*, 867–872. [CrossRef]
19. Zhang, Y.; Liu, Y.; Li, C.; Chen, X.; Wang, Q. Controlled synthesis of Ag_2S quantum dots and experimental determination of the exciton bohr radius. *J. Phys. Chem. C* **2014**, *118*, 4918–4923. [CrossRef]
20. Zhang, X.; Liu, J.; Johansson, E.M.J. Efficient charge-carrier extraction from ag2s quantum dots prepared by the silar method for utilization of multiple exciton generation. *Nanoscale* **2015**, *7*, 1454–1462. [CrossRef] [PubMed]
21. Mir, W.J.; Swarnkar, A.; Sharma, R.; Katti, A.; Adarsh, K.N.V.D.; Nag, A. Origin of unusual excitonic absorption and emission from colloidal Ag_2S nanocrystals: Ultrafast photophysics and solar cell. *J. Phys. Chem. Lett.* **2015**. [CrossRef] [PubMed]
22. Hu, H.; Ding, J.; Zhang, S.; Li, Y.; Bai, L.; Yuan, N. Photodeposition of Ag_2S on TiO_2 nanorod arrays for quantum dot-sensitized solar cells. *Nanoscale Res. Lett.* **2013**, *8*, 10. [CrossRef] [PubMed]
23. Zhang, X.; Liu, J.; Zhang, J.; Vlachopoulos, N.; Johansson, E.M.J. Zno@Ag_2S core-shell nanowire arrays for environmentally friendly solid-state quantum dot-sensitized solar cells with panchromatic light capture and enhanced electron collection. *Phys. Chem. Chem. Phys.* **2015**, *17*, 12786–12795. [CrossRef] [PubMed]
24. Tubtimtae, A.; Wu, K.-L.; Tung, H.-Y.; Lee, M.-W.; Wang, G.J. Ag_2S quantum dot-sensitized solar cells. *Electrochem. Commun.* **2010**, *12*, 1158–1160. [CrossRef]
25. Murray, C.B.; Norris, D.J.; Bawendi, M.G. Synthesis and characterization of nearly monodisperse cde (e = sulfur, selenium, tellurium) semiconductor nanocrystallites. *J. Am. Chem. Soc.* **1993**, *115*, 8706–8715. [CrossRef]
26. Hines, M.A.; Scholes, G.D. Colloidal pbs nanocrystals with size-tunable near-infrared emission: Observation of post-synthesis self-narrowing of the particle size distribution. *Adv. Mater.* **2003**, *15*, 1844–1849. [CrossRef]
27. Zhuang, Z.; Lu, X.; Peng, Q.; Li, Y. A facile "dispersion–decomposition" route to metal sulfide nanocrystals. *Chem. A Eur. J.* **2011**, *17*, 10445–10452. [CrossRef] [PubMed]
28. Zhang, X.; Justo, Y.; Maes, J.; Walravens, W.; Zhang, J.; Liu, J.; Hens, Z.; Johansson, E.M.J. Slow recombination in quantum dot solid solar cell using p-i-n architecture with organic p-type hole transport material. *J. Mater. Chem. A* **2015**, *3*, 20579–20585. [CrossRef]
29. Alfred, J.; Frueh, J. The crystallography of silver sulfide, Ag_2S. *Z. Krist. Cryst. Mater.* **1958**, *110*, 136–144. [CrossRef]

30. Bi, D.; Yang, L.; Boschloo, G.; Hagfeldt, A.; Johansson, E.M.J. Effect of different hole transport materials on recombination in ch3nh3pbi3 perovskite-sensitized mesoscopic solar cells. *J. Phys. Chem. Lett.* **2013**, *4*, 1532–1536. [CrossRef] [PubMed]
31. Lu, L.; Zheng, T.; Wu, Q.; Schneider, A.M.; Zhao, D.; Yu, L. Recent advances in bulk heterojunction polymer solar cells. *Chem. Rev.* **2015**, *115*, 12666–12731. [CrossRef] [PubMed]
32. Ye, M.; Hong, X.; Zhang, F.; Liu, X. Recent advancements in perovskite solar cells: Flexibility, stability and large scale. *J. Mater. Chem. A* **2016**, *4*, 6755–6771. [CrossRef]
33. Sveinbjornsson, K.; Aitola, K.; Zhang, J.; Johansson, M.B.; Zhang, X.; Correa-Baena, J.-P.; Hagfeldt, A.; Boschloo, G.; Johansson, E.M.J. Ambient air-processed mixed-ion perovskites for high-efficiency solar cells. *J. Mater. Chem. A* **2016**, *4*, 16536–16545. [CrossRef]
34. Zhang, X.; Zhang, J.; Liu, J.; Johansson, E.M.J. Solution processed flexible and bending durable heterojunction colloidal quantum dot solar cell. *Nanoscale* **2015**, *7*, 11520–11524. [CrossRef] [PubMed]
35. Etxebarria, I.; Ajuria, J.; Pacios, R. Solution-processable polymeric solar cells: A review on materials, strategies and cell architectures to overcome 10%. *Org. Electron.* **2015**, *19*, 34–60. [CrossRef]
36. Yan, J.; Saunders, B.R. Third-generation solar cells: A review and comparison of polymer:Fullerene, hybrid polymer and perovskite solar cells. *RSC Adv.* **2014**, *4*, 43286–43314. [CrossRef]
37. Li, G.; Zhu, R.; Yang, Y. Polymer solar cells. *Nat. Photonics* **2012**, *6*, 153–161. [CrossRef]
38. Ameri, T.; Min, J.; Li, N.; Machui, F.; Baran, D.; Forster, M.; Schottler, K.J.; Dolfen, D.; Scherf, U.; Brabec, C.J. Performance enhancement of the p3ht/pcbm solar cells through nir sensitization using a small-bandgap polymer. *Adv. Energy Mater.* **2012**, *2*, 1198–1202. [CrossRef]
39. Noh, J.H.; Jeon, N.J.; Choi, Y.C.; Nazeeruddin, M.K.; Gratzel, M.; Seok, S.I. Nanostructured $TiO_2/CH_3NH_3PBI_3$ heterojunction solar cells employing spiro-OMeTAD/co-complex as hole-transporting material. *J. Mater. Chem. A* **2013**, *1*, 11842–11847. [CrossRef]
40. Wang, E.; Hou, L.; Wang, Z.; Hellström, S.; Zhang, F.; Inganäs, O.; Andersson, M.R. An easily synthesized blue polymer for high-performance polymer solar cells. *Adv. Mater.* **2010**, *22*, 5240–5244. [CrossRef] [PubMed]